Modular Toroidal Copper Coil for the Investigation of Inductive Pulsed Power Generators in the MJ-Range

Oliver Liebfried, Volker Brommer, Harald Scharf, Matthias Schacherer, Paul Frings

***Abstract*—Inductive pulsed power generators apply coils as powerful short time energy storage which is an ordinary mean to deliver pulses of high power to loads like electromagnetic accelerators. This article deals with the design, simulation, construction, electrical characterization and a pulsed stress test of a modular toroidal coil. The coil was made from 180 D-shaped copper discs and has an approximate inductance of 1 mH ($f > 50$ Hz) and frequency dependent resistance according to 3.88 m$\Omega \cdot \sqrt{f}$ + 5 mΩ. Its height, diameter and weight is 0.4 m, 1 m and 1 ton respectively. It is designed to store more than 1 MJ of energy.**

***Index Terms*—Pulsed power, inductive storage, skin effect.**

I. Introduction

THERE are several reasons why inductive storages are used within a pulsed power generator for railguns. In combination with a homopolar generator or a battery, the inductor is used to generate the high voltage which is needed to supply railguns with high armature velocities [1]–[3]. In capacitor banks, inductors are used to limit the gradient of the current rise dI/dt and adjust the pulse length to the requirements of the railgun [4]. In combination with batteries, inductors can be considered as a viable possibility to optimize the energy chain and build a more compact pulsed power source than currently available ones [5].

In such a generator, an inductive storage is charged by batteries at low or moderate voltage until a required current maximum. At this time, the current needs to be commutated within few microseconds from the charging circuit to the load circuit by means of opening switches. Corresponding switches are challenging because stray inductances of the circuit generate high voltages according to $U_L = L \cdot dI/dt$. At ISL, thyristors which are turned off by a counter-current pulse were found suitable to meet the challenge and were applied in an XRAM circuit which is used to amplify the charging current. In it, several inductances are charged in series connection and discharged in parallel connection. The suitability of this technique was shown by several small scale demonstrators [5]. Now, the next step is a demonstrator with a stored energy of 1 MJ. This requires a corresponding short-time magnetic energy storage.

This paper reports on the development, construction and tests of a 1 MJ coil for a 20-stage XRAM generator. A goal was an inductance of 1 mH which requires a current of 45 kA to reach 1 MJ.

II. Inductor Design

Inductors are pressure vessels. Its energy density relates directly to the maximum strength σ of the coil material (see eq. 1).

$$W/V = \kappa\sigma \tag{1}$$

Apart from σ, it depends on the form related factor κ. This factor tends toward 1 in case of force balanced coils [6] which can be considered as hybrid between solenoidal and toroidal coil [7]. Energy is stored in the magnetic field of the core and the surroundings. Unfortunately, it is very complicated to produce this kind of coil. Brooks coils, long time known as the coils with the best L-to-R ratio, have a κ of 1/2 and are therefore more compact than toroidal or long solenoidal coils where κ is approximately 1/3 [8], [9]. This compactness is gained by storing a large amount of the energy in the magnetic field around the coil and not inside of them. If high stray fields need to be avoided, shielding has to be applied. But such shielding increases the size of the coil because it has to be placed in a certain distance to the coil in order to prevent saturation of the shielding material [10]. Thus, the size advantage of Brooks coils is lost and toroidal coils are the preferred choice as they encapsulate the magnetic field.

Three principle designs were considered (see Fig. 1): wire wound (1), made from discs (2) or with jelly rolled windings (3). A small DC resistance requires a large wire cross section. Thus, options 2 and 3 are to be preferred in this respect. Both, disc and jelly roll type of a Brooks coil were theoretically investigated by Pokryvailo et al. [11]. They found that the jelly roll type is more efficient due to the skin effect but that the disc type can store more energy because of its higher mechanical strength. A disc type construction was chosen because our workshop allows the production of discs by etching and water jet cutting of copper. Furthermore, most losses will occur during slow charging where the skin effect was believed not to be as pronounced as in the short but high dynamic discharge. A so-called *Shavranov* or *Princeton* D-shape was approximated

Manuscript received September 24, 2019; revised MONTH XX, 2019. This work was supported by the French Government Defense procurement and technology agency (DGA) as part of the ANR Astrid program under Grant ANR-14-ASTR-0025.

O. Liebfried, V. Brommer, H. Scharf and M. Schacherer are with the French-German Research Institute of Saint-Louis (ISL), 5 rue Général Cassagnou, 68301 Saint-Louis, France, e-mail: Oliver.Liebfried@isl.eu, Volker.Brommer@isl.eu, Harald.Scharf@isl.eu, Matthias.Schacherer@isl.eu.

Paul Frings is with the Laboratoire National des Champs Magnétiques Intenses (LNCMI), 143 av. de Rangueil, 31400 Toulouse, France, e-mail: paul.frings@lncmi.cnrs.fr.

(a) wire wound (b) disc (c) jelly roll

Fig. 1. Coil winding topologies

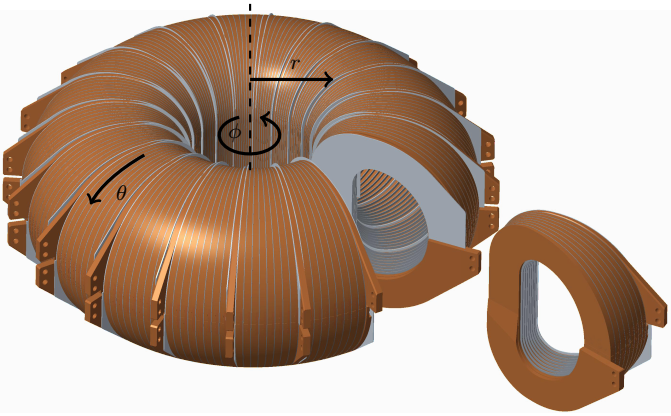

Fig. 2. Simplyfied CAD design of the magnetic storage

for the design because it allows to store 18 % more energy with the same wire length without increasing the mechanical stress [12]. A CAD drawing of the coil design is shown in Fig. 2. Single windings were produced by milling of copper discs. The thickness in toroidal direction (ϕ) of each disc increases from 3 mm to 15 mm. The conductor thickness in radial direction (r) or shell thickness decreases from 85 mm to 75 mm. At the outwards directed side, the disc is cut and a 30 mm wide and 6 mm deep part at each ending was removed. Thus, the endings of the disc can be screwed to the adjacent disc by an additional plate of copper and bending of the discs in toroidal direction. Twenty sub-coils with nine windings each are prepared in such a manner. The outer windings of each sub-coil have terminals at the outer side of the coil. The terminal serves as electrical connector and for mechanical linkage in poloidal (θ) direction. The windings are separated by GRP discs with a thickness of 1.5 mm. The GRP discs between each sub-coil are 2 mm thick and exceed the outer dimension of the copper discs by 5 mm to ensure an electrical insulation of 5 kV. For the same reason, the terminals of the adjacent sub-coils are separated by 16 mm in poloidal direction.

The final coil can be seen in 3.

III. FEM SIMULATION

FEM simulations with *COMSOL Multiphysics*® were performed in order to investigate the electrical characteristics and electromagnetic forces and to gain insight into the current distribution. This was done using the modules *AC/DC: Magnetic Fields* and *Structural Mechanics: Solid Mechanics* in the frequency domain. The number of finite elements (and therefore the simulation time) was reduced by applying simplifications and using the symmetries of the coil design: Only one sub-coil consisting of 9 windings was taken into account

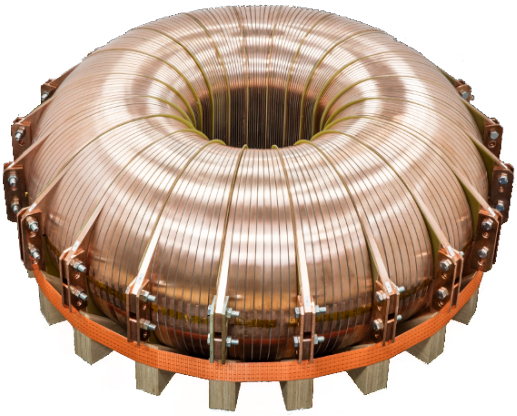

Fig. 3. Assembled toroidal coil

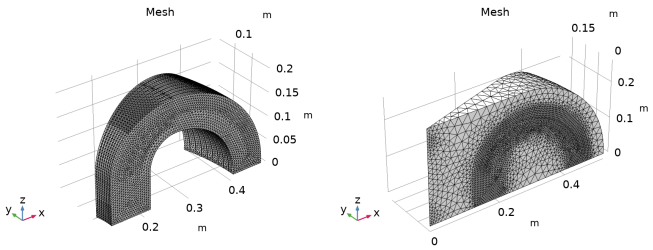

(a) Mesh of coil volume (b) Mesh of air volume

Fig. 4. FEM mesh

exploiting the toroidal symmetry (assuming uniform thickness of 1.5 mm for all GRP discs). Furthermore, the symmetry of the top and bottom halves of the coil can be approximated and used by modeling the windings as straight parts neglecting the pitch angle of 2°. Next, neither the GRP parts between the coil windings nor the connector to the coil were modeled. The GRP is substituted by a corresponding gap between the windings. The generated mesh for the reduced geometry consists of 373642 tetrahedral elements and is outlined in Fig. 4. The settings of the simulation were chosen as follows: In the *Magnetic Fields* module, a *Perfect Magnetic Conductor* boundary condition is applied to the boundaries in toroidal direction (rz-planes). The coil excitation current is introduced at the cut planes of the windings in the manner that it goes from one winding to the next. Additionally, a coil length multiplication factor of two is considered at the geometry analysis step to correct the computation of the coil voltage and resistance. The winding surfaces in the xy-plane and the ones in parallel to the rz-plane were set to the *Roller* boundary condition within the *Solid Mechanics* module for respecting the upper and lower symmetry and considering the mechanical support of the GRP parts.

The inductance and resistance of the coil were estimated for different frequencies by a frequency sweep. The results were multiplied by 20 to consider the total torus and are plotted together with experimental results in Figs. 8 and 9, respectively. An additional stationary study complemented the series for $f = 0$ Hz. For the simulation results presented hereinafter, a frequency of 62.5 Hz and a peak current of

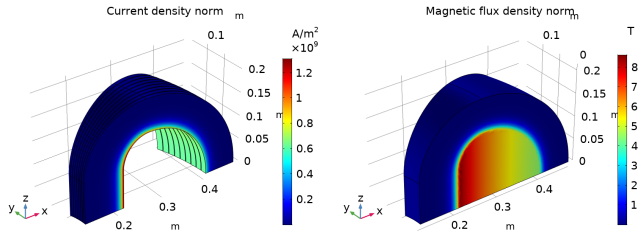

(a) Current density (b) Magnetic flux density

Fig. 5. FEM simulation results

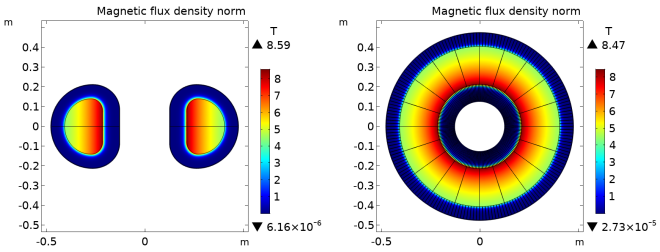

(a) B at vertical cut plane (b) B at horizontal cut plane

Fig. 6. FEM simulation results, duplicated to complete full geometry

50 kA are assumed which match the experimental conditions presented below. The calculated current density and magnetic flux density are displayed in Fig. 5. For a better illustration, simulation results were duplicated at corresponding symmetry axes and shown at a vertical and horizontal cut plane (Fig. 6).

The von Mises stress inside the coil caused by the Lorentz force is shown in Fig. 7 for a coil excitation current of 50 kA. This is equivalent to a stored energy of 1.25 MJ (at L = 1 mH). The maximum stress is 115 MPa which lies far below the 0.2 % proof strength of cold-rolled copper (Cu-OF). The linear relationship between energy and maximum stress allows the estimation of the coil energy limit depending on the used windings material. For 200 MPa, the mechanical limit is reached at 2.2 MJ or 66 kA, respectively.

IV. Coil testing

A. Electrical parameters

The electrical parameters of single sub-coils and the total coil were measured by a micro-ohmmeter (AOIP OM 21) and a LCR-meter (Fluke PM6304). Fig. 8 shows the coil inductance of the total coil and a single sub-coil for frequencies between 50 Hz and 1 kHz in comparison to simulation results. Note, that the frequency scale is given in a quadratic manner. The measured values of the sub-coil were multiplied by a factor of 20 to identify the influence of the coupling between the sub-coils. The inductance of the total toroid is initially 1027 µH at 50 Hz and reaches 950 µH for higher frequencies in an asymptotic behavior. The inductance of the single sub-coil behaves in the same manner although its B-field surrounds the coil (like in a Brooks coil). Note that magnetic coupling increases the inductance by a factor of 2.5.

Fig. 9 shows equivalent measurement results of the coil resistance. The DC value was measured by the micro-ohmmeter.

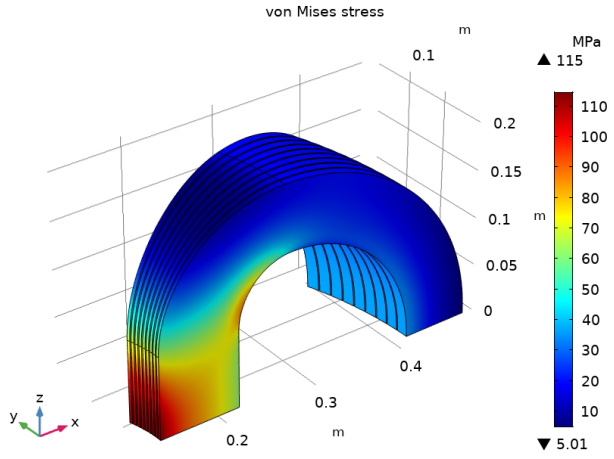

Fig. 7. FEM simulation of the von Mises stress

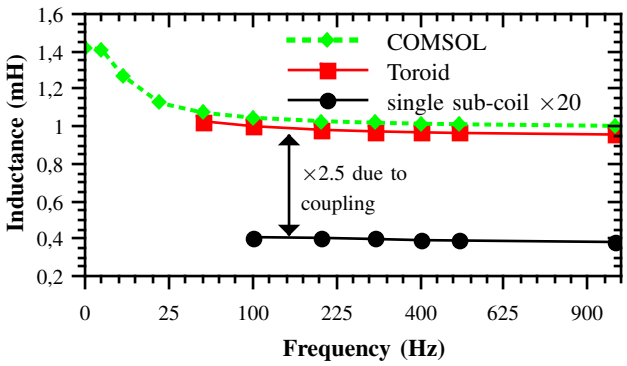

Fig. 8. Measured inductance as function of frequency

The rest by the LCR-meter. Both, the DC resistance of the total coil and the 20-fold resistance of the sub-coil is 5 mΩ. At $f > 0$, the resistance of the total toroid increases linearly with respect to $\sqrt{f}$. The extrapolated resistance of a single coil behaves differently. Its resistance increases less pronounced for small frequencies and becomes also proportional to $\sqrt{f}$ at $f > 300$ Hz ($\approx 17^2\,Hz$). The twenty-fold sub-coil resistance stays constantly around 32 mΩ below that of the torus.

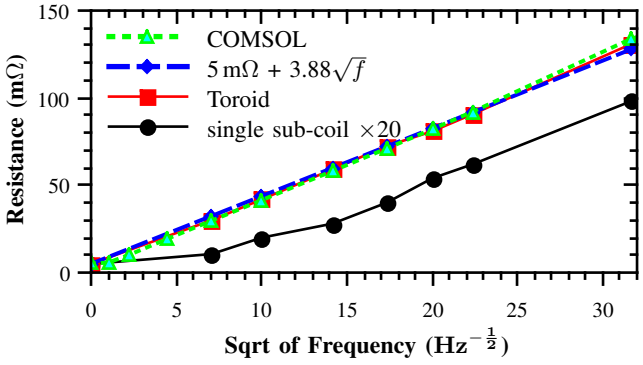

Fig. 9. Measured resistance as function of frequency

Fig. 10. Coil connected to the 10 MJ capacitor bank of PEGASUS at ISL.

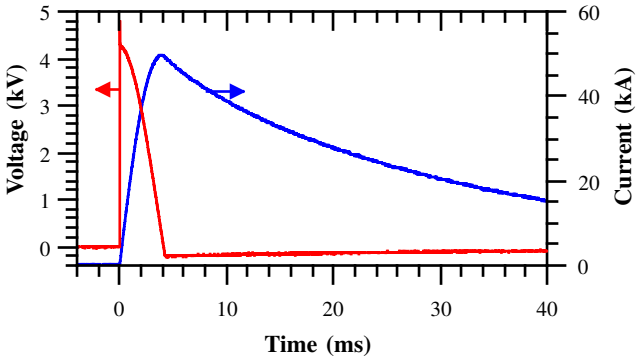

Fig. 11. Measured voltage and current

B. Insulation tests

In future applications, the coil will be charged with all sub-coils in series connection. As result, the highest voltage will appear at the electrical insulation between the first and the last winding. Therefore, the electrical insulation was tested between two disconnected sub-coils. A 50 kV high-voltage power supply with a current limitation of 0.5 mA was used for this purpose. The voltage was step-wise increased and the current was measured in order to identify a voltage breakdown.

Tests revealed various weak spots where the insulation was subsequently strengthened by additional Kapton foils. Finally, a voltage of 6 kV and 7 kV was applied without any breakdown. The tested were stopped after 5 and 2 minutes, respectively.

C. Pulsed stress test

The coil was stress tested by applying a pulsed current generated by the 10 MJ capacitor bank of the railgun facility PEGASUS [4]. Four sub-coils each were connected in series. Five sections were connected in parallel to the capacitor bank (see Fig. 10). The 200 capacitors of PEGASUS with a total capacity of 173 mF were charged to a maximum voltage of 4.3 kV in order to stay below the 5 kV limit of the coil. The capacitors were discharged simultaneously into the coil.

1) I-U measurement: Voltage and current were measured with a HV-voltage probe and a Rogowski coil at one coil interface. Fig. 11 shows the corresponding measurement curves. The current increases within 3.94 ms to its maximum of 50 kA. At this time, Crowbar diodes bypass the capacitors and prevent a ringing of the current. Afterwards the current decays according to a discharge of a RL circuit. The resistive loss energy W_L of the coil was calculated by the voltage signal $U(t)$, the current signal $I(t)$ and the derivative thereof according to

$$W_L = \int_0^{t_{end}} I(t) \cdot \left[U(t) - L \frac{dI(t)}{dt}) \right] dt \qquad (2)$$

The inductance L of the coil was simply set to 1 mH. Thus, W_L was 550 kJ.

2) Magnetic field measurement: The magnetic field was measured by custom made B-dots. B-dots are induction coil sensors which measure the derivative of the magnetic field. The sensor was designed according to [13] with an outer and inner winding diameter of 6 mm and 1.5 mm, respectively. In average, 190 windings of thin copper wire (Ø 0.18 mm) were placed in a 4.3 mm wide groove within a plastic rod. The B-dots were calibrated at the center of a pulsed magnetic field generated by a single loop. The sensitivity of the sensors varied between 450 T/(Vs) and 580 T/(Vs) with an estimated error of 2 %. The signal was filtered by a RC circuit, recorded by an oscilloscope and numerically integrated according to [14] by using the software *Origin*. The rod was simply fixed on a GRP plate by applying a thread on one end. Fig. 12a shows the B-dots installed into the core of the coil. The positions are indicated in Fig. 13. Measured B-field curves are proportional to the current curve and therefore not shown. Instead, the measured peak values are given in Tab. I. The first column gives the number of the B-dot with respect to Fig. 13. The second and third columns give the absolute value and the component in φ-direction, respectively, of the simulated magnetic field at the corresponding positions. The fourth column presents the measured values and the last one presents the deviation between B_{real} and B_φ. The deviation is based on the magnetic field in φ-direction because a B-dot measures only the magnetic field parallel to its axis.

(a) B-dot probes (b) Embedded PT1000s

Fig. 12. GRP insulation disc with sensors

TABLE I
COMPARISON OF MEASUREMENT AND SIMULATION

B-dot	B	B_φ	B_{real}	$\frac{B_\varphi - B_{real}}{B_\varphi} \times 100$
2	4.98 T	4.92 T	4.8 T	2.4 %
4	6.66 T	6.58 T	6.4 T	2.7 %
7	8.04 T	7.95 T	7.5 T	5.7 %
8	8.04 T	7.95 T	7.6 T	4.4 %
10	7.62 T	7.53 T	6.8 T	9.7 %
12	6.64 T	6.55 T	6.3 T	3.8 %

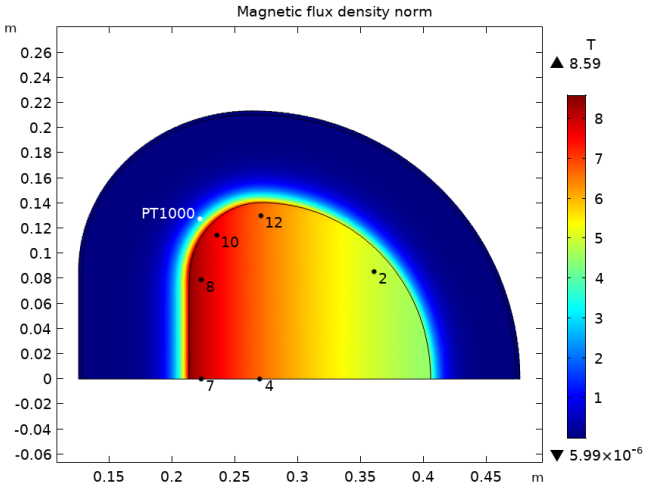

Fig. 13. B-field FEM simulation and measurement probe positions. Numbers relate to the B-dots according Tab. I

Although the measurements are slightly below the simulated values, they confirm the simulated magnetic field distribution shown in Fig. 13. Differences might be due to a certain inaccuracy in sensor placement and orientation. Furthermore, local variation of the magnetic field in toroidal direction is not taken into consideration.

3) Temperature measurement: The coil temperature was measured by installing small PT1000 sensors ($1\times0.8\times3\,mm^3$) into one GRP insulation disc between the windings. Fig. 12b shows a picture of the sensors as they are glued into a groove of the GRP. The signal of one PT1000 was recorded by an oscilloscope via a battery supplied Wheatstone bridge. Its position is indicated in Fig. 13. Fig. 14 shows the corresponding recording from the pulsed stress test over a time of 80 seconds. Note that the applied current pulse is less than 100 ms in comparison. It can be recognized by the short peak at $t = 0$ s due to electromagnetic interference. The blue or dark curve is the smoothed copy of the red or gray one. The temperature increases up to 27.2 °C at $t = 8$ s and subsequently converges toward 26.3 °C at $t > 30$ s. This is a temperature increase of 1.7 ° compared to the initial condition. That the temperature exceeds this value in the beginning can be explained by the position of the sensor and the current distribution in the coil windings. First, the coil heats up at the inner part of the windings where the current flows (see Fig. 13). Afterwards, the heat is diffusing into the copper and thus, it is reduced at the measurement location. The estimated average temperature increase according to equation (3) is 1.4 °.

$$\Delta T = \frac{W_L}{c_p \cdot w} \tag{3}$$

where c_p is the specific heat capacity of the coil material and w is the weight of the coil. The difference between measurement and estimation might be related to measurement errors and the accumulation of it during the integration of I and U and due to local temperature differences within the coil.

4) High-speed camera: A high speed camera was used during the experiment to investigate possible mechanical movements or deformations. Two recorded pictures displayed in an alternating manner are made available on http://ieeexplore.ieee.org as supplementary downloadable material in form of an animated GIF file. One picture was recorded at the beginning and the second one at t = 3.94 ms. Only in this way, the small displacement of the coil windings can be recognized. It can be seen that the coil contracts inwardly, which can be explained by small gaps between the windings due to production tolerances. This movement is seen as uncritical because the coil stabilizes itself by moving toward its axis.

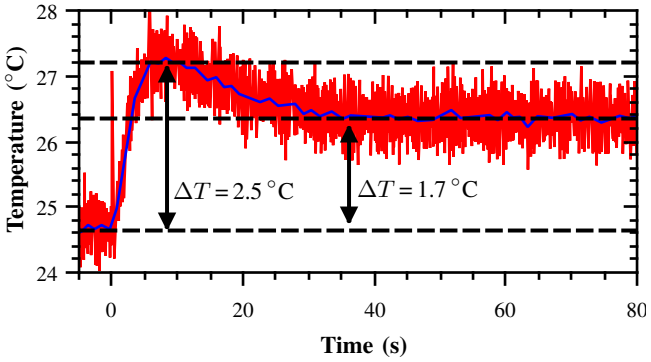

Fig. 14. Temperature measurement

V. Discussion

The construction of a 1 MJ inductive pulse power generator for railguns requires a magnetic storage having a small DC resistance. Production capabilities and concerns regarding the mechanical stability of the coil led to the decision to produce a coil with disc shaped windings. An underestimated characteristic of this design is that the current concentrates at the inner surface of the coil due to the skin effect (see Fig. 5a). Thus, the inductance decreases and the resistance increases remarkably with the frequency (see Figs. 8 and 9). Because the skin depth is proportional to $1/\sqrt{f}$, the resistance depends on the frequency f according to

$$R(f) = R_{DC} + k \cdot \sqrt{f} \tag{4}$$

with DC resistance R_{DC} and the constant term k which includes material and geometrical parameters of the coil. R_{DC} was measured to be 5 mΩ. Variable k was determined by a curve fit in Fig. 9 (blue dashed line) and is 3.88 mΩ. The excellent agreement with the red curve (square measurement points) confirms the existence of the skin effect. The resistance deviation between the total coil and a single sub-coil can be explained by different current distributions: The current is somehow more scattered in case of the sub-coil as the magnetic field is not contained in the core of the coil but more like in a solenoidal coil. Thus, the resistance increase for $f < 300$ Hz is not as high as in case of the completed torus.

The current distribution at the inner surface is in agreement with the FEM simulation (see Fig. 13) which was additionally confirmed by the magnetic field measurement (see Tab. I). The

TABLE II
APPROXIMATION OF COIL RESISTANCE DEPENDING ON PULSE RISE TIME

Frequency	Rise time	Coil resistance	$t_{300K \to 400K}$	cycles
0 Hz	∞	5 mΩ	3.3 s	-
1 Hz	250 ms	8.5 mΩ	3.8 s	15
10 Hz	25 ms	16 mΩ	2 s	80
50 Hz	5 ms	30 mΩ	1 s	200
1 kHz	250 µs	117 mΩ	0.3 s	1200

largest magnetic field appears at the inner surface of the core (straight part of the D). The magnitude of the magnetic field is constant in z-direction and decreases in radial direction. Correspondingly, the largest force is acting on the straight part of the windings which results in the recorded contracting movement of the coil (see animated GIF file). The simulation results in Fig. 7 show that the maximum von Mises stress of approx. 115 MPa appears at the center of the coil (at given simulation conditions). Although the coil should stabilize itself, a supporting cylinder was added for the experiments (see Fig. 10). However, the value is far from the critical value of the used copper which is around 200 MPa. Thus, the stress test until 1.25 MJ did not reveal any mechanical weakness. It suggests that the coil can be charged with a current of up to 66 kA which is equivalent to an energy of 2.2 MJ, respectively. This is well above our goal of 45 kA for the future XRAM generator.

The temperature measurement showed a temperature increased of less than 2 °C. Thus, thermal stress is neglectable in case of high voltage charging as done with the capacitor bank. But as soon as we charge the coil by another energy source than high voltage capacitors, thermal stress will limit the number of repetitions. Tab. II lists some exemplary values for the current rise time and coil resistance according to equation (4), both depending on frequency. Column four gives the time until the coil is heated up from room temperature to 400 K. For 0 Hz, it means that a DC current of 45 kA (equivalent to a stored energy of 1 MJ) can be applied for 3.3 s. In the other cases, the calculated time was doubled to take into account a linear charging behavior. Dividing the heating time (column 4) by the rise time (column 2) shows that several charging cycles or a higher charging current is possible with the coil. It also shows that a shorter charging time is better despite a more pronounced skin effect. More cycles are possible in this case due to lower losses.

VI. CONCLUSION

In conclusion, we built a coil which fulfills our requirements for an inductive pulsed power generator in the MJ-Range. The windings can be re-arranged for different purposes. Thus, XRAM, pulse transformer or single coil arrangements are possible. The coil was tested up to 1.25 MJ without getting close to the mechanical nor the thermal limit of the coil. Based on FEM simulations, the force limit is expected at 2.2 MJ. The thermal limit depends strongly on the charging time, but several repetitions are possible before the coil heats up by 100 K. Thus, the coil provides a more than sufficient safety margin with respect to forces and heating. Another design (jelly roll or wire wound) would be better with respect to the skin effect which affects the resistance as well as the inductance of the coil already at very small frequencies. Finally, Tab. III summarizes the specifications of the coil.

TABLE III
MEASURED COIL SPECIFICATIONS

No. of segments	20
Outer diameter	960 mm
..with connectors	1030 mm
Inner diameter	260 mm
Height	423 mm
Volume	2201
Weight	1050 kg
DC resistance	5 mΩ
Inductance @ 50 Hz	1 mH
Energy density @ 45 kA	4.5 MJ/m^3
Specific energy @ 45 kA	1 kJ/kg

ACKNOWLEDGMENT

We acknowledge the help of Bernhard Grasser and all of those who helped in the preparation of the coil.

REFERENCES

[1] D. Hackworth, D. Deis, P. Eckels, and D. Marschik, "A 10 MJ cryogenic inductor," *IEEE Trans. Magn.*, vol. 22, no. 6, pp. 1495–1498, Nov. 1986.
[2] A. Pokryvailo, "Development of long-charge inductive storage systems at Soreq NRC," in *15th IEEE Int. Pulsed Power Conf. (PPPS). Dig. Techn. Pap.*, Monterey, US-CA, 2005, pp. 100–103.
[3] J. B. Cornette, J. D. Sterrett, J. R. Lippert, and R. W. Williams, "Final design and commissioning test results for the hypervelocity launcher research complex battery power supply," in *7th IEEE Int. Pulsed Power Conf. (PPPS). Dig. Techn. Pap.*, 1989, pp. 131–133.
[4] E. Spahn, M. Lichtenberger, and F. Hatterer, "Pulse forming network for the 10 MJ-railgun PEGASUS," in *Proc. 5th Europ. Symp. Electromagn. Launch Techn.*, Toulouse, France, Apr.10-13 1995.
[5] O. Liebfried and V. Brommer, "A four-stage XRAM generator as inductive pulsed power supply for a small-caliber railgun," *IEEE Trans. Plasma Sci.*, vol. 41, no. 10, pp. 2805–2809, Oct. 2013.
[6] A. Badel, "Superconducting magnetic energy storage using high temperature superconductor for pulse power supply," Ph.D. dissertation, INPG, Université de Grenoble, Sep. 2010. [Online]. Available: http://tel.archives-ouvertes.fr/tel-00654844
[7] S. Nomura, N. Watanabe, C. Suzuki, H. Ajikawa, M. Uyama, S. Kajita, Y. Ohata, H. Tsutsui, S. Tsuji-Iio, and R. Shimada, "Advanced configuration of superconducting magnetic energy storage," *Energy*, vol. 30, no. 11–12, pp. 2115–2127, 2005.
[8] F. C. Moon, "The virial theorem and scaling laws for superconducting magnet systems," *Journal of Applied Physics*, vol. 53, no. 12, pp. 9112–9121, 1982.
[9] Y. Eyssa and R. Boom, "Considerations of a large force balanced magnetic energy storage system," *IEEE Trans. Magn.*, vol. 17, no. 1, pp. 460–462, Jan 1981.
[10] A. Pokryvailo, I. Ziv, and M. Shapira, "Repetitive inductive storage supply for an ETC tank gun," *IEEE Trans. Magn.*, vol. 39, no. 1, pp. 257–261, Jan. 2003.
[11] A. Pokryvailo, M. Kanter, and N. Shaked, "Discharge efficiency of cylindrical storage coils," *IEEE Transactions on Magnetics*, vol. 32, no. 2, pp. 497–504, Mar 1996.
[12] P. Birkner, "Toroide mit idealem Feld," *Electrical Engineering (Archiv fur Elektrotechnik)*, vol. 74, no. 4, pp. 275–287, 1991.
[13] S. Tumanski, "Induction coil sensors-a review," *Measurements Science and Technology*, vol. 18, pp. R31–R46, 2007. [Online]. Available: stacks.iop.org/MST/18/R31
[14] J. Wey, D. Eckenfels, C. Gauthier, and R. Charon, "High accuracy measurements on railguns," *Magnetics, IEEE Transactions on*, vol. 31, no. 1, pp. 764–769, Jan 1995.